



**Manchester
Metropolitan
University**

Kamal, Surabhi and Balu, Sridharan and Palanisamy, Selvakumar and Kasi-
mayan, Uma and Velusamy, Vijayalakshmi and Yang, Thomas CK (2019) *Syn-
thesis of boron doped C₃N₄/NiFe₂O₄ nanocomposite: An enhanced visible
light photocatalyst for the degradation of methylene blue*. Results in Physics.
ISSN 2211-3797

Downloaded from: <http://e-space.mmu.ac.uk/622104/>

Publisher: Elsevier

DOI: <https://doi.org/10.1016/j.rinp.2019.01.004>

Usage rights: Creative Commons: Attribution-Noncommercial-No Deriva-
tive Works 4.0

Please cite the published version

<https://e-space.mmu.ac.uk>

Accepted Manuscript

Synthesis of boron doped $C_3N_4/NiFe_2O_4$ nanocomposite: An enhanced visible light photocatalyst for the degradation of methylene blue

Surabhi Kamal, Sridharan Balu, Selvakumar Palanisamy, Kasimayan Uma, Vijayalakshmi Velusamy, Thomas C.K. Yang

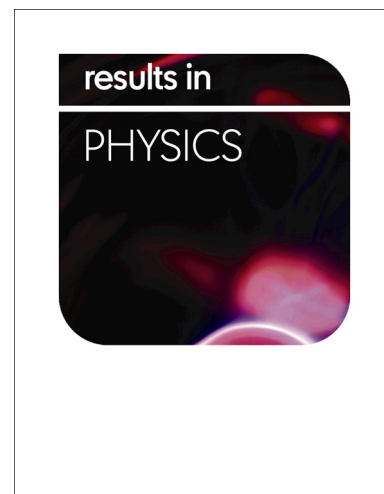
PII: S2211-3797(18)33086-9
DOI: <https://doi.org/10.1016/j.rinp.2019.01.004>
Reference: RINP 1970

To appear in: *Results in Physics*

Received Date: 21 November 2018
Revised Date: 27 December 2018
Accepted Date: 2 January 2019

Please cite this article as: Kamal, S., Balu, S., Palanisamy, S., Uma, K., Velusamy, V., Yang, T.C.K., Synthesis of boron doped $C_3N_4/NiFe_2O_4$ nanocomposite: An enhanced visible light photocatalyst for the degradation of methylene blue, *Results in Physics* (2019), doi: <https://doi.org/10.1016/j.rinp.2019.01.004>

This is a PDF file of an unedited manuscript that has been accepted for publication. As a service to our customers we are providing this early version of the manuscript. The manuscript will undergo copyediting, typesetting, and review of the resulting proof before it is published in its final form. Please note that during the production process errors may be discovered which could affect the content, and all legal disclaimers that apply to the journal pertain.



Synthesis of boron doped $C_3N_4/NiFe_2O_4$ nanocomposite: An enhanced visible light photocatalyst for the degradation of methylene blue

Surabhi Kamal^a, Sridharan Balu^a, Selvakumar Palanisamy^{a, b*}, Kasimayan Uma^c, Vijayalakshmi Velusamy^b, Thomas C.K. Yang^{a, c**}

^aDepartment of Chemical Engineering and Biotechnology, National Taipei University of Technology, Taipei, Taiwan-106.

^bDivision of Electrical and Electronic Engineering, School of Engineering, Manchester Metropolitan University, Chester Street, Manchester M1 5GD, United Kingdom.

^c Precision Analysis and Materials Research Centre, National Taipei University of Technology, Taipei, Taiwan-106.

*Corresponding authors: S. Palanisamy (prmselva@gmail.com; prmselva@mail.ntut.edu.tw); T.C.K. Yang (ckyang@mail.ntut.edu.tw)

Abstract

In this paper, we report the synthesis of boron doped $C_3N_4/NiFe_2O_4$ nanocomposite and its application as a visible-light photocatalyst for the degradation of methylene blue (MB). Boron-doped C_3N_4 (BCN) was prepared by simple thermal condensation of dicyandiamide with boric acid, and $NiFe_2O_4$ nanoparticles were prepared by the simple sol-gel method. The as-synthesized nanocomposite materials were characterized and confirmed by the X-ray diffraction spectroscopy, Fourier-transform infrared spectroscopy, field-emission scanning electron microscopy, transmission electron microscopy, UV-Visible diffuse reflectance spectroscopy, X-ray photoelectron spectroscopy, and photoluminescence spectroscopy. The photocatalytic activity of BCN/ $NiFe_2O_4$ nanocomposite was evaluated towards the degradation of MB in the presence of visible light irradiation. The obtained results confirmed that BCN/ $NiFe_2O_4$ composite has higher degradation efficiency (98%) than that of BCN and $NiFe_2O_4$.

Keywords: Thermal condensation; Sol-gel method; BCN/ $NiFe_2O_4$ nanocomposite; Visible-light photocatalyst; Methylene blue.

Introduction

The major environmental issues are directly caused by the growth of industrialization with increasing world population leading to depletion of air, soil and water systems [1]. The untreated waste and pollutants discharged from these industries have a high concentration of organic contaminants, salts, dyes, and heavy metals [2]. Among all, dyes and pigments are considered as toxic pollutants due to their harmful effect on to the hydrosphere, agriculture and living organisms [3]. Furthermore, the dye-containing effluents are more stable and non-biodegradable due to its complex structure [4]. To date, different methods have been employed to remove the dyes such as photocatalysis [5, 6], catalytic treatment [7] and chemical treatment [8]. Over the past few decades, the semiconductor photocatalytic technology has emerged as an alternate procedure for the elimination of organic pollutants and to make the pollutant mineralize into CO₂ and H₂O [9].

Carbon nitride (g-C₃N₄) is a well-known semiconductor material, has attracted much attention in a wide range of fields due to its high chemical stability [10], low cost [11], less toxicity [12] and significant bandgap (2.7-2.8 eV) [10]. More recently, g-C₃N₄ incorporated metals [13, 14], metal oxides [13, 15] and non-metals [13, 16] have shown enhanced photocatalytic performance towards the degradation organic dyes than pristine g-C₃N₄. Also, the introduction of non-metals such as boron or sulfur has maintained the metal-free nature of g-C₃N₄ because of their high ionization energy and high electronegativity [17]. Among different non-metals, boron is a lightweight element and forms a stable chemical bond with the g-C₃N₄ [18]. Due to the discussed unique properties, it can often alter the photocatalytic activity of g-C₃N₄ when combined with other semiconductor materials [19]. The useful addition of semiconductor materials into the boron doped g-C₃N₄ (BCN) matrix can reduce the energy band gap and electronic structure which may eventually increase the electron-hole separation and the catalytic activity [20]. More recently, the spinel ferrite structures (MFe₂O₄, M=Zn, Ni, Co) have found significant interest in the application of organic dye degradation [5, 21] and water splitting reactions [22, 23]. In particular, nickel ferrite (NiFe₂O₄) is a well-known visible-light semiconductor and having a

narrow band gap of 2.19 eV with decent photocatalytic stability [24]. Recent studies revealed that the photocatalytic activity of C_3N_4 had been improved in the visible light region when combined with noble metal and metal oxides [25]. The heterojunction structure of the semiconductor composites is the main reason for the enhanced photocatalytic activity. However, $NiFe_2O_4$ decorated BCN nanocomposite has never been used for the photocatalytic applications. Given the above points, the integration of unique properties of BCN with $NiFe_2O_4$ could enhance the photocatalytic activity of organic dyes than that of the pure BCN and $NiFe_2O_4$.

In this present work, we report the synthesis of BCN/ $NiFe_2O_4$ nanocomposite for the first time. The as-prepared BCN/ $NiFe_2O_4$ nanocomposite was used as a novel visible-light catalyst for the photodegradation of organic dye, and methylene blue (MB) was used as a model dye for the photocatalytic measurements. The photocatalytic activity of BCN, $NiFe_2O_4$ and BCN/ $NiFe_2O_4$ towards the degradation of MB was studied and discussed in detail. The photocatalytic degradation mechanism of MB using the photocatalyst has also been discussed.

Experimental

Materials

Iron chloride ($FeCl_3$, 98%, Alfa Aesar, WH, USA), nickel chloride ($NiCl_2 \cdot 6H_2O$, Sigma Aldrich, MO, USA), boric acid (H_3BO_3 , J.T. Baker, CV, PA), dicyandiamide ($C_2H_4N_4$, 99%, Alfa Aesar, UK), sodium hydroxide (NaOH, Nihon Shiyaku Industries Ltd., Taiwan) and double distilled water was used throughout the experiment. All chemicals used in this work were of analytical grade and were used as received.

Synthesis of BCN

BCN was prepared by thermal polycondensation reaction using dicyandiamide and boric acid [25]. Briefly, 1.68 g of dicyandiamide and 0.6 g of boric acid were evenly grounded using an agate mortar. Further, this mixture was placed into a crucible with a lid and heated in a muffle furnace at 550

°C for 3h with a heating rate of 5°C min⁻¹. The final powder was collected, washed with ethanol followed by water and dried in an oven for 5 hr at 80°C.

Preparation of BCN/NiFe₂O₄ nanocomposite

The following procedure was used for the preparation of BCN/NiFe₂O₄ nanocomposite. First, the dispersion of BCN (1 g) in 100 mL water was prepared using ultra-sonication method (30 min). About 1 M of NiCl₂ and 2 M of FeCl₃·9H₂O was added into the above dispersion with continuous stirring. The pH of the solution was maintained at pH~13 using 3 M NaOH. Then, the emulsion was stirred for 1 h at 80°C using magnetic stirrer and dried at 90°C. The obtained powder was calcined for 3h at 450°C with a heating rate of 5°C min⁻¹. The obtained sample was labeled as BCN/NiFe₂O₄ nanocomposite. The similar procedure was used for the preparation of the NiFe₂O₄ and was prepared without BCN.

Characterization

The structural patterns and crystallite size of the synthesized materials were analyzed by the X-ray diffractometer (XRD) PANalytical X'Pert PRO instrument with CuK α radiation ($\lambda=1.5418$ Å). The surface morphology and elemental analysis of as-synthesized nanocomposite materials were analyzed using a JEOL-JEM2100F transmission electron microscopy (TEM) and JEOL JSM-7100F field-emission scanning electron microscope (FESEM). Fourier-transform infrared (FT-IR) spectra were obtained by Perkin Elmer FT-IR spectrometer. The FT-IR sample pellets were prepared using KBr substrate with synthesized different materials. UV-visible diffuse reflectance spectra (UV-DRS) was analyzed using Cary 5000 UV-Vis-NIR spectrophotometer with an integrating sphere attachment. A spectralon blank was used as the reference. The X-ray photoelectron spectroscopy (XPS) was analyzed by JEOL JPS-9030. Photoluminescence (PL) spectroscopy was measured using Dongwoo-Ramboss 500i, Gyeonggi-Do, Korea.

Photodegradation Experiments

For the degradation experiments, the MB was used as a model textile pollutant to evaluate the catalytic performance of as-synthesized materials. The Mercury-Xenon lamp (350 W, 0.33 mW cm⁻²,

Prosper Technology, Taiwan) light was used as a visible light source. For the experiment, 100 mL of MB (5 ppm) dye was mixed with 100 mg of BCN/NiFe₂O₄ nanocomposite. Before the light introduction, the above mixture was stirred for 30 minutes to obtain dye-catalyst adsorption equilibrium. At a preset time (5 min), about 4 mL of the dispersion was drawn and filtered for the UV measurements.

Results and discussion

Characterization of the as-synthesized materials

The structural and phase information of all the samples were characterized by XRD. **Fig. 1A** shows the two distinct diffraction peaks for typical BCN at 26.9° and 43.8° which can be indexed as (002) and (100) planes (JCPDS card No. 34-0421) [26]. The significant broad peak at (002) attributes to the higher inter-planar distance like boron nitride and graphite. The plane (100) is due to the in-plane reflections of BCN [27, 28]. The diffraction peak pattern of NiFe₂O₄ detected at 30.15°, 35.65°, 44.49°, 51.95°, 57.24° and 62.96° which are designated by their corresponding indexes 220, 311, 400, 422, 511 and 440 respectively (JCPDS 74-2081) [24]. The peaks at 26.74°, 35.65°, 44.49°, 51.95°, 57.24°, 62.96° can be ascribed to the (002, 220, 311, 400, 422, 511 and 440) of BCN/NiFe₂O₄ nanocomposite. The results confirmed the successful formation of BCN/NiFe₂O₄ nanocomposite.

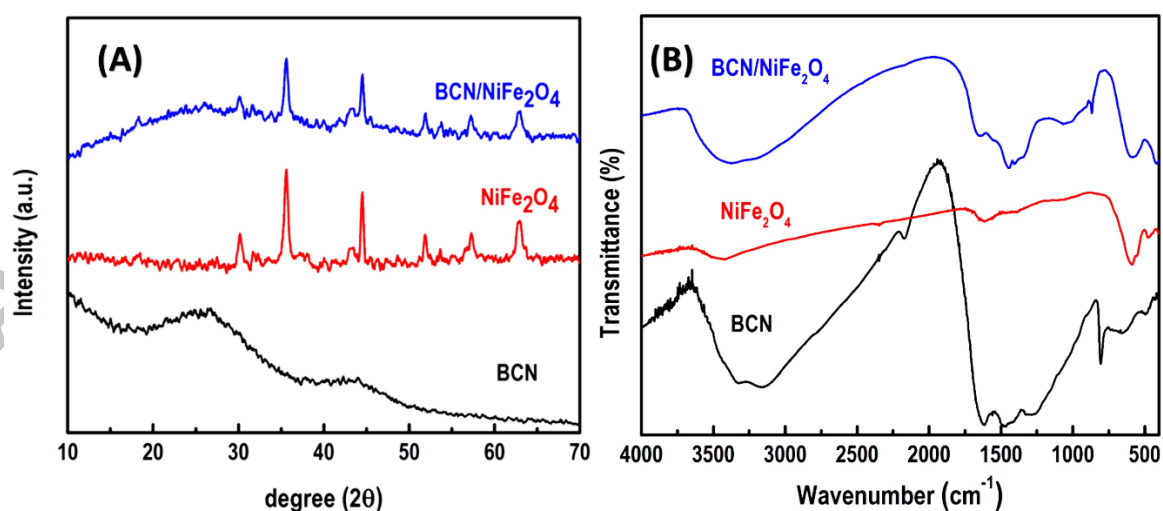


Fig. 1 A) XRD patterns of as-synthesized BCN, NiFe₂O₄ and BCN/NiFe₂O₄ nanocomposite. B) FT-IR spectra of BCN, NiFe₂O₄ and BCN/NiFe₂O₄ nanocomposite.

The FT-IR spectra of BCN, NiFe₂O₄ and BCN/NiFe₂O₄ nanocomposites are shown in **Fig. 1B**. The NiFe₂O₄ and BCN/NiFe₂O₄ nanocomposite shows a broad vibration band at 3100-3500 cm⁻¹ and is due to the stretching vibrations of N-H or O-H group. The peaks in BCN from 1200 to 1700 cm⁻¹ can be attributed from the vibrational stretching band of C-N and C=N, and the peak around 806 cm⁻¹ shows the band of triazine units [29]. The peaks of in-plane B-N and B-C are observed at 1462 and 1273 cm⁻¹ respectively [30, 31]. In NiFe₂O₄, the stretching vibrations of Fe-O bonds in tetrahedral positions and metal-O bonds in octahedral positions shows the sharp peak at 592 cm⁻¹ and a weak peak at 466 cm⁻¹ respectively [32]. For BCN/NiFe₂O₄ nanocomposite, the bands at 1652, 1450 and 579 cm⁻¹ assigned to BCN, B-N vibration and Fe-O bonds respectively. The result confirmed that the structure of BCN and NiFe₂O₄ remains unchanged in the nanocomposite.

The surface morphology of the synthesized materials was analyzed by the FESEM, and the corresponding FESEM images are shown in **Fig. 2**. In **Fig. 2A**, a rough sheet-like structure was observed for BCN. **Fig. 2B** shows the aggregated particles of NiFe₂O₄ with the average diameter around 100 nm. This variable size of the particles is due to the synthesis process including milling in an agate mortar [33]. **Fig. 2C** represents the BCN/NiFe₂O₄ nanocomposite with aggregated NiFe₂O₄ nanoparticles embedded on the sheet-like BCN. The size of the NiFe₂O₄ nanoparticles was reduced after incorporated with BCN than primary NiFe₂O₄ particles. The reduced size of the nanoparticles is may be due to the presence of more surface area and photogenerated electrons and holes of BCN. The elemental analysis (**Fig. 2D**) and elemental mapping (**Fig. 2 (E-J)**) results of the BCN/NiFe₂O₄ nanocomposite confirmed the presence of C, O, B, Ni, N, and Fe.

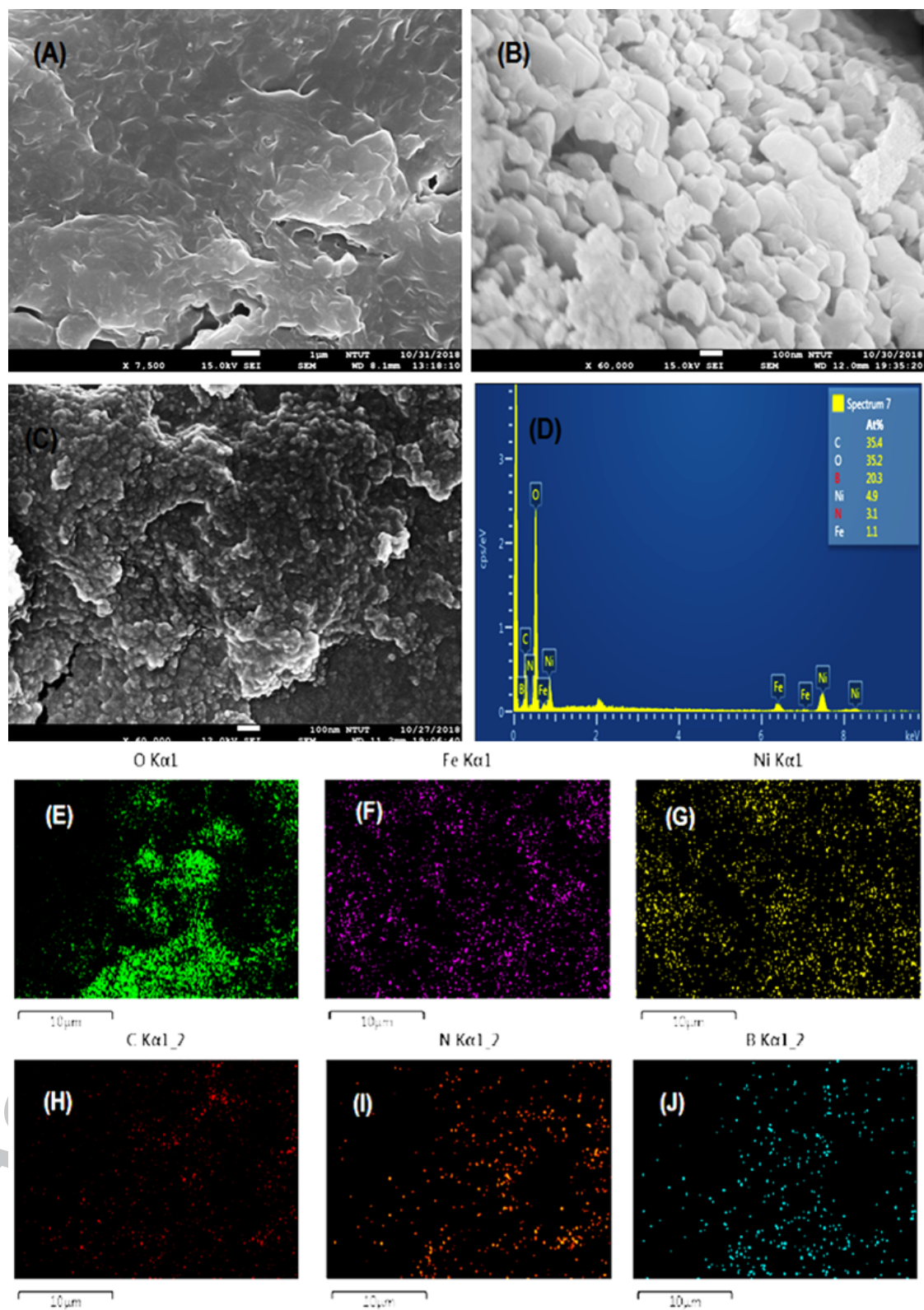


Fig. 2 FESEM images of BCN (A), NiFe₂O₄ (B), BCN/NiFe₂O₄ nanocomposite (C) and elemental analysis (D) and elemental mapping of O, Fe, Ni, C, N, and B (E-J) on BCN/NiFe₂O₄ nanocomposite.

TEM was also performed to examine the structural morphology of as-prepared BCN, NiFe₂O₄ and BCN/NiFe₂O₄ nanocomposite. **Fig. 3** shows the TEM images of BCN (A), NiFe₂O₄ (B) and BCN/NiFe₂O₄ nanocomposite (C). **Fig. 3A** shows the sheet-like structure of BCN and the agglomerated NiFe₂O₄ nanoparticles are visible in **Fig. 3B**. **Fig. 3C** confirmed that NiFe₂O₄ nanoparticles embedded on the surface of BCN. The obtained TEM images of BCN, NiFe₂O₄ and BCN/NiFe₂O₄ nanocomposite has found to similar to the morphology of FESEM.

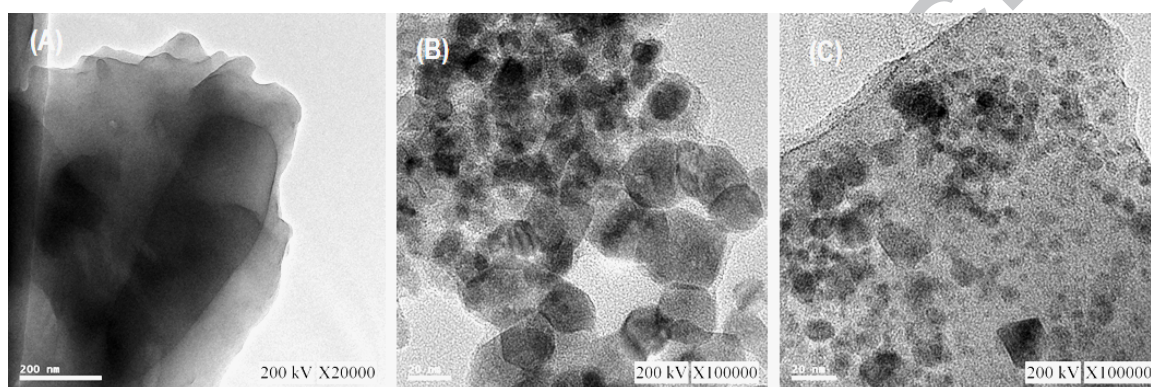


Fig. 3 TEM images of BCN (A), NiFe₂O₄ (B) and BCN/NiFe₂O₄ nanocomposite (C).

The UV-DRS of the as-prepared composite material were measured in the wavelength ranges between 200 and 800 nm. **Fig. 4A** shows the UV-DRS of BCN, NiFe₂O₄ and BCN/NiFe₂O₄ nanocomposite. The BCN and NiFe₂O₄ show the band edge wavelengths in the visible light region of 200-800 nm. It can be seen that the band edge of the BCN/NiFe₂O₄ nanocomposite increases compared with BCN and NiFe₂O₄ which indicates the effective absorption of visible light by the BCN/NiFe₂O₄ nanocomposite than others. **Fig. 4B** shows the indirect bandgap of BCN/NiFe₂O₄ nanocomposite about 2.05 eV, and it was lower than that of BCN (2.65 eV) and NiFe₂O₄ (2.38 eV).

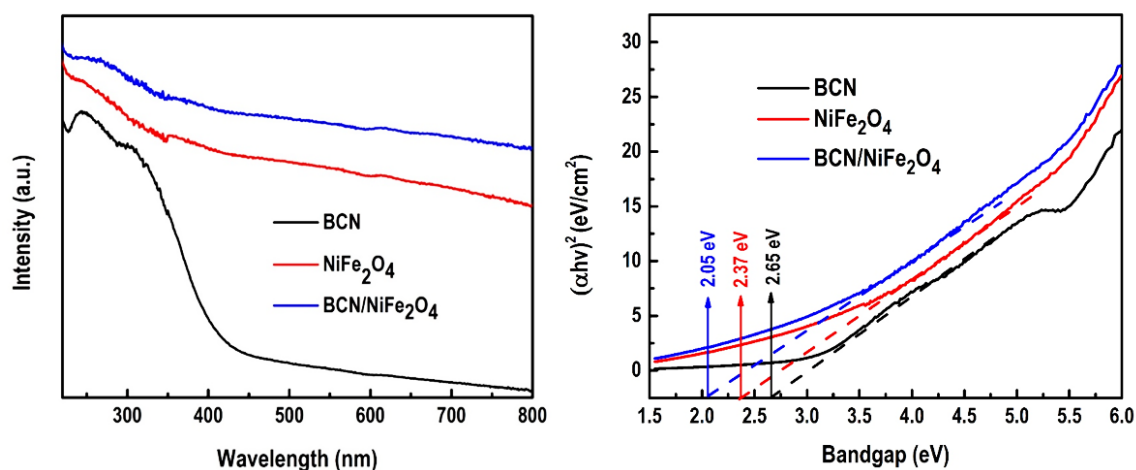


Fig. 4 UV-DRS of BCN, NiFe₂O₄ and BCN/NiFe₂O₄ nanocomposite (A), the indirect band gap of as-prepared BCN, NiFe₂O₄ and BCN/NiFe₂O₄ nanocomposite (B).

The surface elemental composition and the electronic state of the BCN/NiFe₂O₄ nanocomposite were characterized by XPS analysis and is shown in **Fig. 5**. The binding energies of B 1s, C 1s, N 1s, Ni 2p, Fe 2p and O 1s of the nanocomposite are shown in **Fig. 5 (A-F)**. The characteristic peak at 191.2 eV reveals the binding energy of B 1s and confirms the presence of B-N [34]. A broad peak of C1s includes C-C, C-O, C-N and C-B components appeared at binding energies of 284.9 eV, 288.4 eV, 285.6 eV, and 283.8 eV respectively [35]. The N 1s spectrum also includes the binding energies to pyridinic nitrogen at 398.6 eV, C-N-H group at 399.5 eV and graphitic nitrogen at 400.7 eV [36]. The binding energy of Ni 2p_{3/2} appears at 856.9 eV, and Ni 2p_{1/2} appears at 875.1 eV [37]. For the binding energy of Fe 2p appeared at 711.1 eV and attributed to Fe 2p_{3/2}. The peak at 724.4 eV indicates the presence of Fe 2p_{1/2} [38]. The characteristic peak at 532.5 eV shows the O 1s in the NiFe₂O₄ composite at which is assigned for the O²⁻ and spinel metal oxides [38].

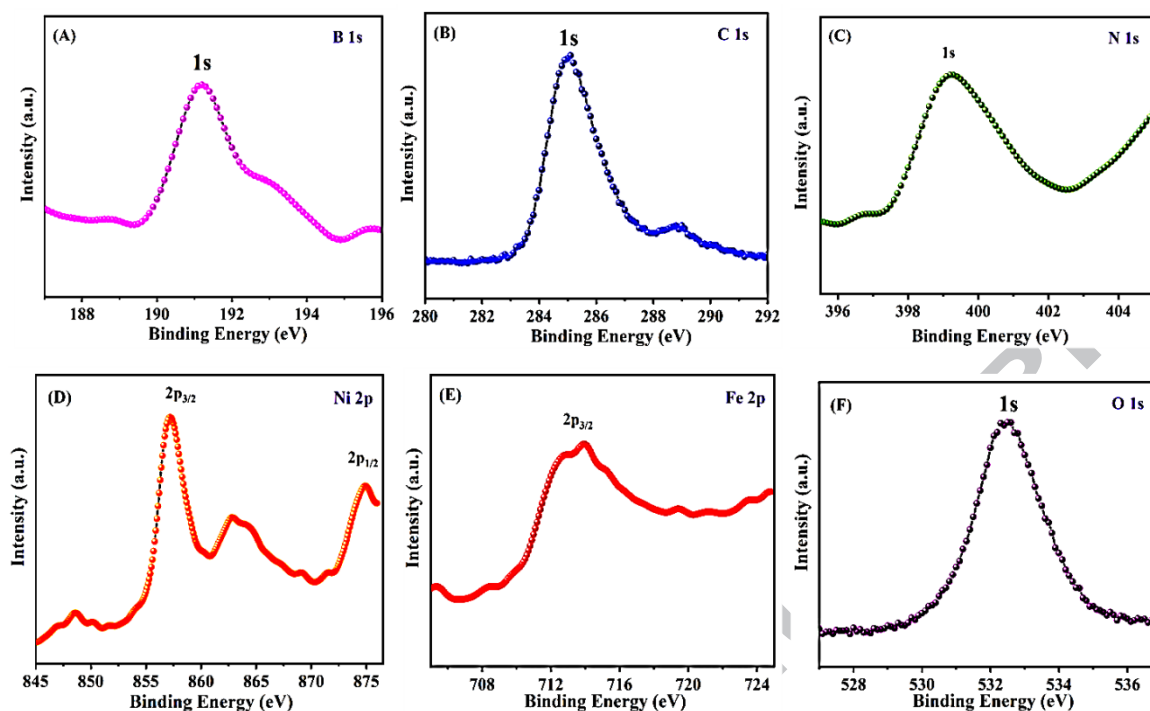


Fig. 5 High-resolution XPS spectra (B 1s, C 1s, N 1s, Ni 2p, Fe 2p, and O 1s) of as-synthesized BCN/NiFe₂O₄ nanocomposite.

Photoluminescence spectroscopy

The PL spectra of BCN/NiFe₂O₄, NiFe₂O₄, and BCN, are shown in **Fig. 6**. A broad peak at 415 nm is observed for the BCN which exhibits the higher recombination rate of electron-hole pairs. **Fig. 6 inset** shows the reduced PL intensities of NiFe₂O₄ and BCN/NiFe₂O₄ which infers a significant reduction in the recombination rate when compared to BCN. There is a decrease in the emission peak intensity of BCN/NiFe₂O₄ which also indicates the effective e⁻/h⁺ charge separation and increases the transfer efficiency from the valence band to the conduction band. Further, NiFe₂O₄ nanoparticles incorporated with BCN behaves as an electron acceptor and thus increases the photocatalytic activity.

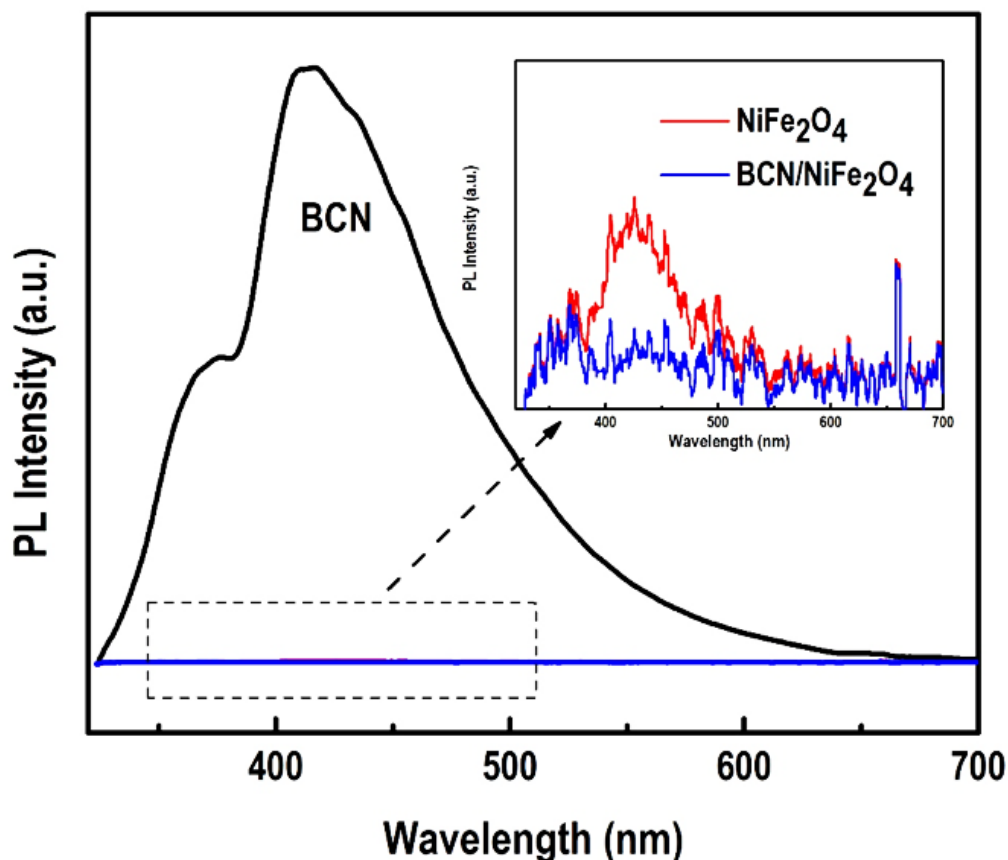


Fig. 6 PL spectra of BCN and NiFe_2O_4 , BCN/ NiFe_2O_4 nanocomposite (inset)

Photo-catalytic degradation of MB

Fig. 7A shows the photo-catalytic degradation of MB by the as-prepared nanocomposite in the presence of visible light irradiation at a different time. It can be seen that the decrease in intensity at 664 nm with the increasing the visible light irradiation time. The result indicates the effective photodegradation of MB by the BCN/ NiFe_2O_4 nanocomposite. A plot of time vs. the percentage of dye remaining in the solution is shown in **Fig. 7B**. The obtained results revealed that the degradation efficiencies of 25.6, 69 and 98% were obtained using NiFe_2O_4 , BCN and BCN/ NiFe_2O_4 nanocomposites at 80 min.

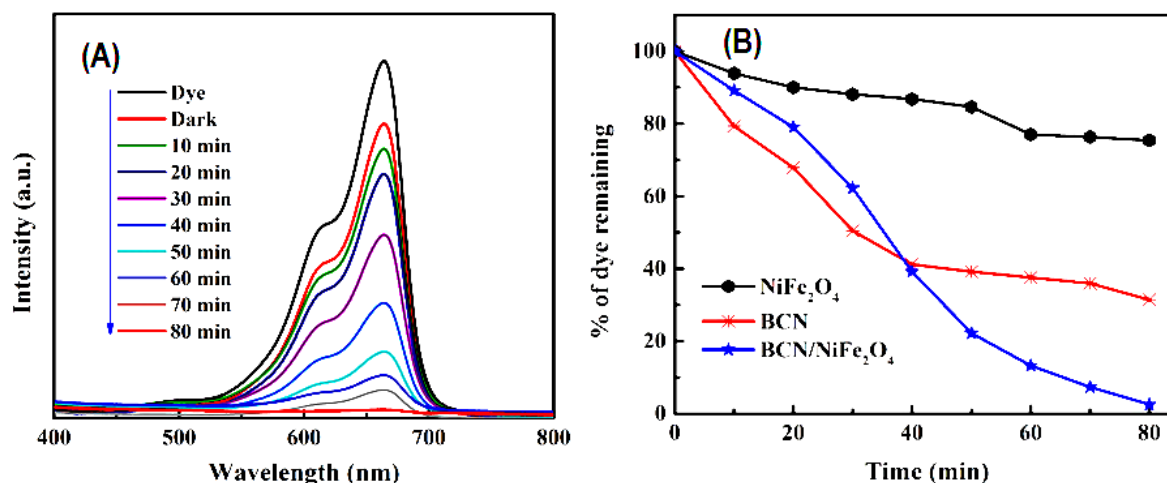
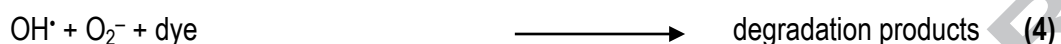
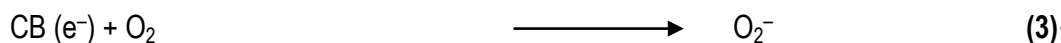
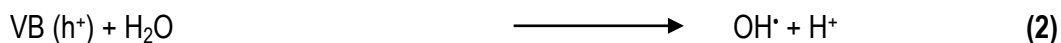
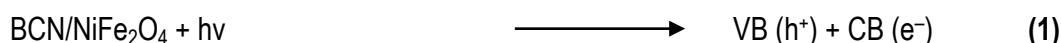


Fig. 7 Photocatalytic degradation of MB in the presence of BCN/NiFe₂O₄ nanocomposite (A). A plot of time vs. % of dye remaining in the solution (B).

Photodegradation mechanism of MB

The synergistic effect between BCN and NiFe₂O₄ results in the enhance the photocatalytic activity and higher adsorption of MB on the catalyst surface. As discussed earlier that the as-synthesized nanocomposite has lower bandgap (2.05 eV) than that of BCN (2.65 eV) and NiFe₂O₄ (2.38 eV). The lower bandgap of the BCN/NiFe₂O₄ nanocomposite will help to achieve the enhanced photocatalytic activity towards the degradation of MB. Also, the recombination rate of BCN was reduced upon composite with NiFe₂O₄, and resulting in the higher electron-hole separation and a considerable population of e⁻/h⁺ pairs. The migration of electrons from the CB of BCN to the CB of NiFe₂O₄ causes a high negative (e⁻) rich environment which also makes slightly positive VB of NiFe₂O₄. The holes on the VB of NiFe₂O₄ migrate to VB of BCN simultaneously. This process of redistribution of electrons-holes delays the recombination rate of the photoinduced carriers. The increased recombination rate of electrons and holes could reduce the catalytic activity due to the lack of producing OH[•] and O₂^{•-}. When the reaction medium introduced into the visible light irradiation, the valence band (VB) electrons were excited to the conduction band (CB), this photogenerated e⁻ and h⁺ involved in the production of OH[•] and O₂^{•-} radicals. The as-formed OH[•] and O₂^{•-} radicals can oxidize the MB into the degradation

products such as CO_2 and H_2O . The mechanism of the photodegradation of dye can be expressed by the following equations (Eqn. 1–4).



The kinetics and rate constant of the photocatalytic degradation reaction using NiFe_2O_4 , BCN and $\text{BCN/NiFe}_2\text{O}_4$ are shown in **Fig. 8A**. A plot of $\ln(C/C_0)$ vs. time follows the pseudo-first order kinetics. The rate constant (k') value of $\text{BCN/NiFe}_2\text{O}_4$ nanocomposite ($k'=4.4 \times 10^{-2} \text{ min}^{-1}$) was obtained from the intercept of the linear line which was 12.7 times greater than NiFe_2O_4 ($k'=3.5 \times 10^{-3} \text{ min}^{-1}$) and 3.2 times greater than that of BCN ($k'=1.4 \times 10^{-2} \text{ min}^{-1}$). The correlation coefficient (R^2) values of BCN, NiFe_2O_4 and $\text{BCN/NiFe}_2\text{O}_4$ nanocomposite materials are found to be 0.9608, 0.9595 and 0.9796 respectively.

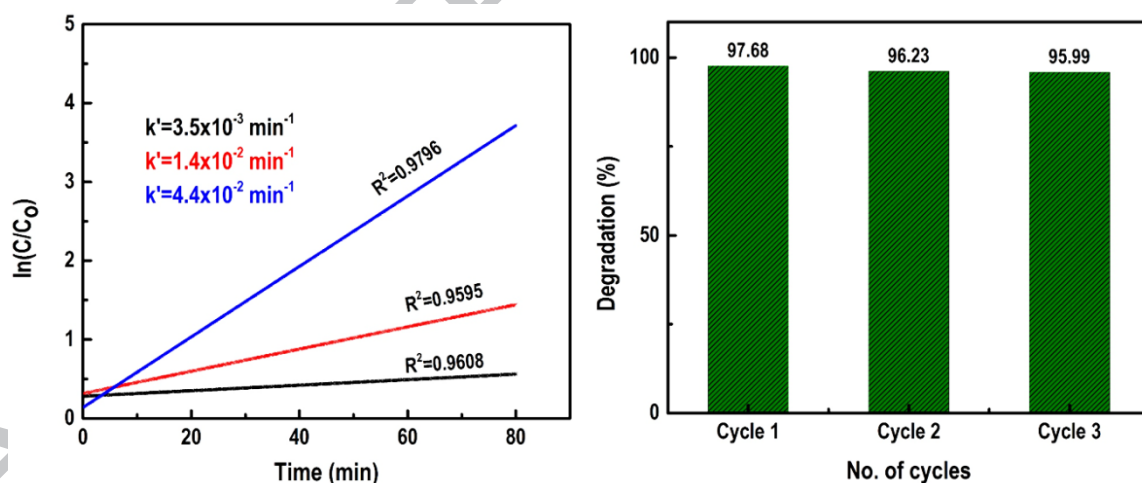


Fig. 8 A) Pseudo-first order kinetics of photodegradation using NiFe_2O_4 (a), BCN (b), $\text{BCN/NiFe}_2\text{O}_4$ (c), and reusability of $\text{BCN/NiFe}_2\text{O}_4$ nanocomposite (B).

Reusability

The economic feasibility and practical usability of a photocatalyst material are analyzed with the reusability studies. Hence, the reusability studies of the $\text{BCN/NiFe}_2\text{O}_4$ nanocomposite are shown in **Fig.**

8B. After the degradation, the catalyst nanocomposite was collected by centrifugation. Then, it was washed with deionized water and ethanol to remove the adsorbed MB molecules and dried in an oven for 3 h. The collected nanocomposite was used subsequently to measure the photocatalytic efficiency. From the obtained results, the percentage degradation of MB was calculated to be 97.68%, 96.23% and 95.99% for three successive cycles. The result indicates the excellent cyclic stability of the BCN/NiFe₂O₄ nanocomposite.

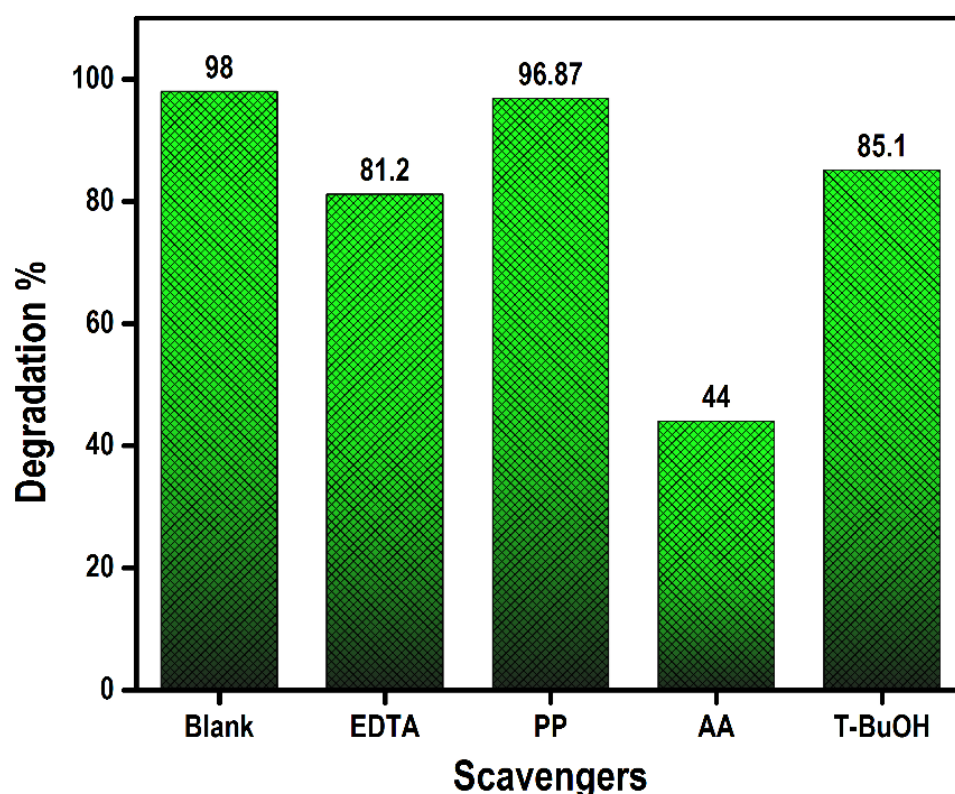


Fig. 9 Degradation % of MB using BCN/NiFe₂O₄ nanocomposite in the presence of different scavenging species (scavengers).

To understand the role of the active species generated during the photocatalytic reaction, ethylenediaminetetraacetic acid (EDTA), K₂S₂O₈ (PP), acrylamide (AA) and tertiary butyl alcohol (T-BuOH) were used as the scavenger materials to trap holes (h⁺), electrons (e⁻), superoxide radicals (•O₂⁻) and hydroxyl radicals (•OH) respectively. The degradation process without scavengers shows 98% of MB degradation after 80 min. After the addition of EDTA, PP, AA, and T-BuOH scavengers into the system, the degradation percentage of MB was 81.2, 96.87, 44.0 and 85.1% respectively (**Fig. 9**). The

results indicate that the contribution of active species in the photodegradation of MB as in the order of $\bullet\text{O}_2^- > \bullet\text{OH} > \text{h}^+ > \text{e}^-$. Therefore, the degradation of MB significantly reduced because of the addition of AA to capture the $\bullet\text{O}_2^-$. On the other hand, the degradation percentage of MB slightly decreased when PP, T-BuOH, and EDTA were added to the system.

Conclusion

In conclusion, a novel BCN/NiFe₂O₄ photocatalyst was prepared by simple thermal condensation and sol-gel methods for the first time. The synthesized materials were confirmed by different physicochemical techniques. The as-synthesized nanocomposite material was used for the effective degradation of MB. The obtained results revealed that BCN/NiFe₂O₄ nanocomposite had better catalytic activity towards MB than that of pristine NiFe₂O₄ and BCN. The degradation of the MB was confirmed by intensity variations of its UV absorption peaks, and the obtained results confirmed the pseudo-first-order kinetics mechanism. As a future perspective, the synthesized BCN/NiFe₂O₄ nanocomposite can be used as a low-cost photocatalyst material for the applications of environmental decontamination of organic dyes.

Conflicts of interest

The authors confirm that there are no conflicts to declare.

Acknowledgments

The authors would like to thank the Precision Analysis and Materials Research Centre, National Taipei University of Technology, Taipei, Taiwan for the financial support to this research.

References

- [1] Houas, H. Lachheb, M. Ksibi, E. Elaloui, C. Guillard, J.-M. Herrmann, Photocatalytic degradation pathway of methylene blue in water, *Appl. Catal. B*, 31 (2001) 145–157.
- [2] S.B. Bukallah, M. Rauf, S. AlAli, Removal of methylene blue from aqueous solution by adsorption on sand, *Dyes Pigm.*, 74 (2007) 85–87.
- [3] U.G. Akpan, B.H. Hameed, Parameters affecting the photocatalytic degradation of dyes using TiO_2 -based photocatalysts: a review, *J. Hazard. Mater.*, 170 (2009) 520–529.
- [4] Cripps, J.A. Bumpus, S.D. Aust, Biodegradation of azo and heterocyclic dyes by *Phanerochaete chrysosporium*, *Appl. Environ. Microbiol.*, 56 (1990) 1114–1118.
- [5] S. Balu, K. Uma, G.-T. Pan, T. Yang, S. Ramaraj, Degradation of methylene blue dye in the presence of visible light using $\text{SiO}_2@ \alpha\text{-Fe}_2\text{O}_3$ nanocomposites deposited on SnS_2 flowers, *Materials*, 11 (2018) 1030.
- [6] K. Uma, S. Balu, G.-T. Pan, T. Yang, Assembly of ZnO nanoparticles on $\text{SiO}_2@ \alpha\text{-Fe}_2\text{O}_3$ nanocomposites for an efficient Photo-Fenton reaction, *Inorganics*, 6 (2018) 90.
- [7] Namasivayam, D. Kavitha, Removal of Congo Red from water by adsorption onto activated carbon prepared from coir pith, an agricultural solid waste, *Dyes Pigm.*, 54 (2002) 47–58.
- [8] H. Métivier-Pignon, C. Faur-Brasquet, P. Le Cloirec, Adsorption of dyes onto activated carbon cloths: approach of adsorption mechanisms and coupling of ACC with ultrafiltration to treat coloured wastewaters, *Sep. Purif. Technol.*, 31 (2003) 3–11.
- [9] F. Han, V.S.R. Kambala, M. Srinivasan, D. Rajarathnam, R. Naidu, Tailored titanium dioxide photocatalysts for the degradation of organic dyes in wastewater treatment: a review, *Appl. Catal. A.*, 359 (2009) 25–40.
- [10] J. Wen, J. Xie, X. Chen, X. Li, A review on g-C₃N₄-based photocatalysts, *Appl. Surf. Sci.*, 391 (2017) 72–123.

- [11] Y. Zhang, J. Liu, G. Wu, W. Chen, Porous graphitic carbon nitride synthesized via direct polymerization of urea for efficient sunlight-driven photocatalytic hydrogen production, *Nanoscale*, 4 (2012) 5300–5303.
- [12] G. Dong, Y. Zhang, Q. Pan, J. Qiu, A fantastic graphitic carbon nitride (g-C₃N₄) material: electronic structure, photocatalytic and photoelectronic properties, *J. Photochem. Photobiol., C*, 20 (2014) 33–50.
- [13] G. Mamba, A. Mishra, Graphitic carbon nitride (g-C₃N₄) nanocomposites: a new and exciting generation of visible light driven photocatalysts for environmental pollution remediation, *Appl. Catal., B*, 198 (2016) 347–377.
- [14] M. Zhang, X. Bai, D. Liu, J. Wang, Y. Zhu, Enhanced catalytic activity of potassium-doped graphitic carbon nitride induced by lower valence position, *Appl. Catal., B*, 164 (2015) 77–81.
- [15] P. Xia, B. Zhu, B. Cheng, J. Yu, J. Xu, 2D/2D g-C₃N₄/MnO₂ nanocomposite as a direct Z-scheme photocatalyst for enhanced photocatalytic activity, *ACS Sustainable Chem. Eng.*, 6 (2017) 965–973.
- [16] Y. Deng, L. Tang, G. Zeng, Z. Zhu, M. Yan, Y. Zhou, J. Wang, Y. Liu, J. Wang, Insight into highly efficient simultaneous photocatalytic removal of Cr (VI) and 2, 4-dichlorophenol under visible light irradiation by phosphorus doped porous ultrathin g-C₃N₄ nanosheets from aqueous media: performance and reaction mechanism, *Appl. Catal., B*, 203 (2017) 343–354.
- [17] L. Jiang, X. Yuan, Y. Pan, J. Liang, G. Zeng, Z. Wu, H. Wang, Doping of graphitic carbon nitride for photocatalysis: a review, *Appl. Catal., B*, 217 (2017) 388–406.
- [18] F. Hou, Y. Li, Y. Gao, S. Hu, B. Wu, H. Bao, H. Wang, B. Jiang, Non-metal boron modified carbon nitride tube with enhanced visible light-driven photocatalytic performance, *Mater. Res. Bull.*, 110 (2019) 18–23.

- [19] Y. Hou, Z. Wen, S. Cui, X. Guo, J. Chen, Constructing 2D porous graphitic C₃N₄ nanosheets/nitrogen-doped graphene/layered MoS₂ ternary nanojunction with enhanced photoelectrochemical activity, *Adv. Mater.*, 25 (2013) 6291–6297.
- [20] Y. Liu, Y. Song, Y. You, X. Fu, J. Wen, X. Zheng, NiFe₂O₄/g-C₃N₄ heterojunction composite with enhanced visible-light photocatalytic activity, *J. Saudi Chem. Society*, 22 (2018) 439–448.
- [21] G. Zhao, L. Liu, J. Li, Q. Liu, Efficient removal of dye MB: Through the combined action of adsorption and photodegradation from NiFe₂O₄/Ag₃PO₄, *J. Alloys Compd.*, 664 (2016) 169–174.
- [22] N. Gokon, H. Murayama, A. Nagasaki, T. Kodama, Thermochemical two-step water splitting cycles by monoclinic ZrO₂-supported NiFe₂O₄ and Fe₃O₄ powders and ceramic foam devices, *Sol. Energy*, 83 (2009) 527–537.
- [23] Friebel, M.W. Louie, M. Bajdich, K.E. Sanwald, Y. Cai, A.M. Wise, M.-J. Cheng, D. Sokaras, T.C. Weng, R. Alonso-Mori, Identification of highly active Fe sites in (Ni, Fe) OOH for electrocatalytic water splitting, *JACS*, 137 (2015) 1305–1313.
- [24] T. Peng, X. Zhang, H. Lv, L. Zan, Preparation of NiFe₂O₄ nanoparticles and its visible-light-driven photoactivity for hydrogen production, *Catal. Commun.*, 28 (2012) 116–119.
- [25] S. Zhang, P. Gu, R. Ma, C. Luo, T. Wen, G. Zhao, W. Cheng, X. Wang, Recent developments in fabrication and structure regulation of visible-light-driven g-C₃N₄-based photocatalysts towards water purification: A critical review, *Catal. Today*, (2018) <https://doi.org/10.1016/j.cattod.2018.09.013>.
- [26] J. Pang, Y. Chao, H. Chang, H. Li, J. Xiong, M. He, Q. Zhang, H. Li, W. Zhu, Tuning electronic properties of boron nitride nanoplate via doping carbon for enhanced adsorptive performance, *J. Colloid Interface Sci.*, 508 (2017) 121–128.
- [27] X. Liu, Y. Gao, M. Zhang, X. Zhang, S. Wang, B. Feng, Synthesis of fluorescent BCN hybrid nanosheets: A highly efficient fluorosensor for rapid, simple, sensitive Ag⁺ detection, *RSC Adv.*, 5 (2015) 52452–52458.

- [28] E.D. Rivera-Tapia, C.A. Fajardo, Á.J. Ávila-Vega, C.F. Ávila, F.M. Sánchez-Arévalo, I. Chango-Villacís, F.J. Quiroz-Chávez, J. Santoyo-Salazar, R.C. Dante, Synthesis of boron carbon nitride oxide (bcno) from urea and boric acid, *Fullerenes, Nanotubes and Carbon nanostructures*, 24 (2016) 8–12.
- [29] W. Lei, D. Portehault, R. Dimova, M. Antonietti, Boron carbon nitride nanostructures from salt melts: tunable water-soluble phosphors, *JACS*, 133 (2011) 7121–7127.
- [30] A. Prakash, S.D. Nehate, K.B. Sundaram, Boron carbon nitride based metal-insulator-metal UV detectors for harsh environment applications, *Opt. Lett.*, 41 (2016) 4249–4252.
- [31] D.H. Kim, E. Byon, S. Lee, J.-K. Kim, H. Ruh, Characterization of ternary boron carbon nitride films synthesized by RF magnetron sputtering, *Thin Solid Films*, 447 (2004) 192–196.
- [32] H.Y. Zhu, R. Jiang, S.H. Huang, J. Yao, F.Q. Fu, J.B. Li, Novel magnetic NiFe₂O₄/multi-walled carbon nanotubes hybrids: facile synthesis, characterization, and application to the treatment of dyeing wastewater, *Ceram. Int.*, 41 (2015) 11625–11631.
- [33] Moeinpour, A. Alimoradi, M. Kazemi, Efficient removal of Eriochrome black-T from aqueous solution using NiFe₂O₄ magnetic nanoparticles, *J. Environ. Health Sci. Eng.*, 12 (2014) 112.
- [34] W. Tian, Q. Shen, N. Li, J. Zhou, Efficient degradation of methylene blue over boron-doped g-C₃N₄/Zn_{0.8}Cd_{0.2}S photocatalysts under simulated solar irradiation, *RSC Adv.*, 6 (2016) 25568–25576.
- [35] M. Florent, T.J. Bandoz, Irreversible water mediated transformation of BCN from a 3D highly porous form to its nonporous hydrolyzed counterpart, *J. Mater. Chem. A*, 6 (2018) 3510–3521.
- [36] S. Zhang, L. Gao, D. Fan, X. Lv, Y. Li, Z. Yan, Synthesis of boron-doped g-C₃N₄ with enhanced electro-catalytic activity and stability, *Chem. Phys. Lett.*, 672 (2017) 26–30.
- [37] X. Li, L. Wang, L. Zhang, S. Zhuo, A facile route to the synthesis of magnetically separable BiOBr/NiFe₂O₄ composites with enhanced photocatalytic performance, *Appl. Surf. Sci.*, 419 (2017) 586–594.

[38] S. Huang, Y. Xu, M. Xie, H. Xu, M. He, J. Xia, L. Huang, H. Li, Synthesis of magnetic $\text{CoFe}_2\text{O}_4/\text{g-C}_3\text{N}_4$ composite and its enhancement of photocatalytic ability under visible-light, *Colloids and Surfaces A: Physicochem. Eng. Aspects*, 478 (2015) 71–80.

Highlights

- For the first time, $\text{BCN}/\text{NiFe}_2\text{O}_4$ nanocomposite has been used for the photocatalytic degradation of organic dye.
- MB has been used as a model organic dye to study the photocatalytic behavior of synthesized nanomaterials.
- The photocatalyst can able to degrade 98% of MB within 80 min under visible light irradiation.
- The $\text{BCN}/\text{NiFe}_2\text{O}_4$ nanocomposite has enhanced photocatalytic activity towards MB than that of BCN and NiFe_2O_4 .
- The as-synthesized nanocomposite photocatalyst had excellent cyclic stability.